Impedance-based stability analysis and comparison of different grid-forming control approaches

Alexander Bisseling*, Pascal Weber*, Philipp Frank, Joschua Moser, Michael Suriyah, Thomas Leibfried
Karlsruhe Institute of Technology
Karlsruhe, Germany
*alexander.bisseling@kit.edu, pascal.weber@kit.edu

***Abstract*—This paper presents an impedance-based analysis and comparison of three grid-forming control approaches derived from the synchronous generator swing equation and implemented for an E-STATCOM in EMT simulations. The study considers a synchronverter and two virtual synchronous machine concepts that differ in their virtual stator representation, namely virtual admittance and virtual impedance. The results show that the virtual-admittance-based approaches exhibit very similar dynamic and impedance characteristics, whereas the virtual-impedance-based approach deviates significantly. In addition, the effect of integrating a notch filter into the virtual admittance control structure is analyzed by evaluating the resulting frequency-dependent impedance. Finally, all three control approaches are assessed with respect to their compliance with German grid code requirements.**

***Index Terms*—grid-forming control, frequency-dependent impedance, passivity-based stability analysis, E-STATCOM, EMT**

I. Introduction

In the course of the energy transition and the corresponding loss of inertia of large generators the need for grid-forming (GFM) inverter-based resources (IBR) providing a virtual counterpart increases rapidly. To achieve the needed GFM behavior, the IBR must not only be equipped with a sufficient energy storage or connected to a dc link which provides the required energy, but also a corresponding GFM control approach. In the past, several control approaches have been proposed, discussed and validated, such as the droop-based [1], [2] or matching control [3], [4], the virtual synchronous machine (VSM) and the synchronverter (SV). In this paper, the focus lies on the VSM and the SV approach. The VSM approach aims to emulate the inertia behavior of a synchronous generator (SG) using the power-related swing equation while controlling the reactive power and ac terminal voltage independently from the active power. Several VSM control variants have been investigated in contributions like [5]–[7]. This contribution will study the behavior of two of these variants that differ in their virtual stator representation. The SV approach equals the VSM in terms of an emulation of a SG whereby the physical presentation of the behavior of a SG is considered more in detail, resulting in a coupled active and reactive power control. The SV has been introduced by [8] and enhanced as well as adapted in contributions like [7], [9]–[11].

To ensure compatibility with the grid and hence, a stable and reliable grid operation the behavior of IBRs and their GFM control must be investigated thoroughly. This includes not only the GFM behavior and the provision of inertia itself as described exemplarily in the German Technical Requirements for grid-forming assets [12] but also stability aspects related to non-power frequencies like sub- and supersynchronous stability as well as harmonic stability as defined in [13]. There are several approaches to evaluate and analyze the non-power frequency related stability, often simply referred to as harmonic stability, including analyzes in the time domian, the frequency domain as well as Eigenvalue-based stability analyzes [14], [15]. In the frequency domain, the impedance-based stability analysis, in combination with the passivity-based assessment, allows a straightforward evaluation of the system's behavior at the point of common coupling (PCC) [16]–[18].

In this contribution, a modular multilevel converter (MMC)-based static synchronous compensator with ancillary energy storage (E-STATCOM) either controlled by a VSM control approach with a virtual impedance (VSM-Z), a VSM control approach with a virtual admittance (VSM-Y) or a SV control approach is simulated in electromagnetic transients (EMT) software. Subsequently, the respective frequency-dependent impedance of each approach is determined by means of a frequency scan. The impedances are evaluated in terms of their small signal behavior and passivity over a wide frequency range. Subsequently, the different approaches and their effect on the frequency-dependent impedance are discussed.

This paper is structured as follows: Section 2 provides an introduction and an overview of the E-STATCOM model and the considered GFM control approaches. In section 3 the time domain results are shown and discussed, whereas in section 4 the frequency dependent impedances of the three approaches are evaluated and compared to each other. Section 5 summarizes the results and concludes this contribution.

II. IBR model and control approaches

The following section describes the analyzed E-STATCOM model and the control approaches under investigation. Figure 1 provides an overview of the E-STATCOM and the three GFM ac-side control approaches considered.

A. E-STATCOM model

The design and configuration of the E-STATCOM model is based on the MMC-based double star bridge cell (DSBC)

979-8-3315-8138-1

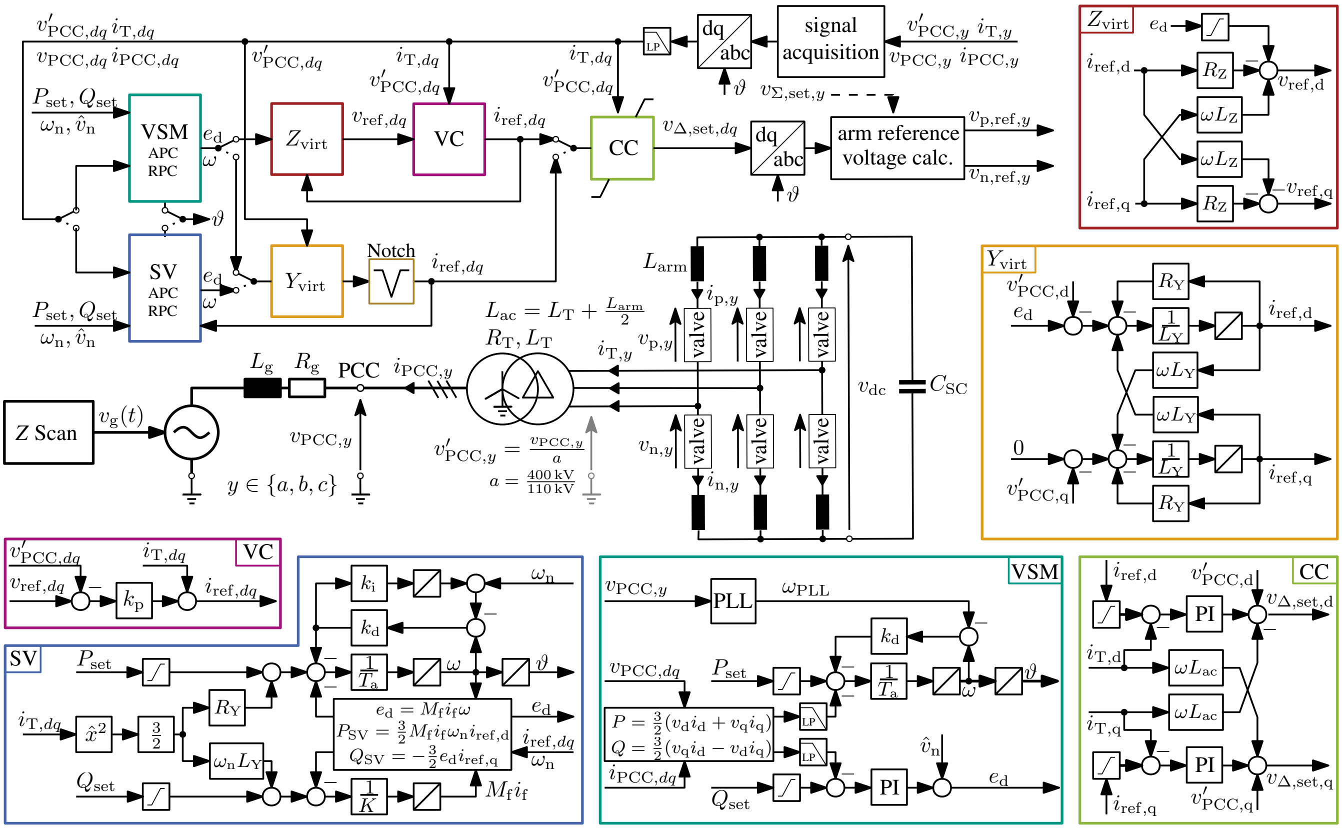

Fig. 1: Overview of the E-STATCOM and the three considered GFM control approaches

approach with ancillary supercapacitor storage on the dc side, similar to [19]. Table I summarizes the parameters of the considered system. The MMC is modeled as averaged voltage source model where each arm consists of a voltage source and an equivalent arm capacitance aggregating the submodule capacitances (Type 5, see [20]) to track and control the stored energy in each MMC arm. The inner current control ensures a vertical and horizontal energy balance while the energy of the submodules is balanced through ancillary energy storage at the converter's dc side avoiding a constraint throughout an arbitrary ac-side contingency. However, the ancillary energy storage is balanced through the ac side but with a lower controller bandwidth to reduce the influence on the transient ac-side dynamics [19]. Note that the inner current control and dc-side control are not considered in the figure and result in the manipulated variable $v_{\Sigma,\text{set},y}$.

TABLE I: Parameter set of considered E-STATCOM

Parameter	Variable	Value
Grid parameters	R_g, L_g	5.837 Ω, 186 mH
	v_grid, ω_n	400 kV, 2π·50 Hz
	SCR, $\frac{X}{R}$	SCR = 9, $\frac{X}{R}$ = 10
E-STATCOM parameters	S_r, P_r	300 MVA, 150 MW
	$v_{\text{r,PCC}}/v_{r,\text{T}}$	400 kV / 110 kV
	$v_{\text{r,dc}}$, $C_{\text{r,SC}}$	50 kV, 475 mF
	R_ac, R_Y, R_Z	0.08 Ω, 0.24 Ω, 0 Ω
	L_ac, L_Y, L_Z	0.038 H, 0.049 H, 0.037 H

B. GFM control approaches

Figure 1 gives an overview of the three considered GFM control approaches controlling the ac side of the E-STATCOM. All three approaches have the following in common: a limited current controller CC, the signal acquisition, low pass filtering and the transform in the rotating dq reference frame. In the following, the differences between the three GFM control approaches will be discussed:

1) SV: The Synchronverter has been introduced by [8] and later adapted and enhanced in [9], [10], [21]. It aims to mimic a synchronous generator and considers not only the power-based swing equation but also the coupling of active and reactive power due to the magnetic coupling of the field windings and current. As a result of its self-synchronizing behavior, there is no need for a phase-locked loop (PLL) for resynchronization. The swing equation provides the virtual rotor angle ϑ and the internal angular frequency ω. The reactive power controller and the coupling equations result in the virtual internal voltage e_d, which is subsequently used by the virtual admittance Y_virt for calculating the reference currents $i_{\text{ref},dq}$. Since a dc voltage offset in the ac voltage leads to a 50 Hz oscillation in dq frame, $i_{\text{ref},dq}$ is additionally filtered by a notch filter with a base frequency of 50 Hz to mitigate this oscillation (see [7]). The filter is implemented as a 4^{th} order Butterworth bandstop filter with a Q factor of Q=2, denoting the ratio of the base frequency to the bandwidth.

2) VSM-Y: The VSM approach is also based on the swing equation emulating the inertia behavior of a synchronous

979-8-3315-8138-1

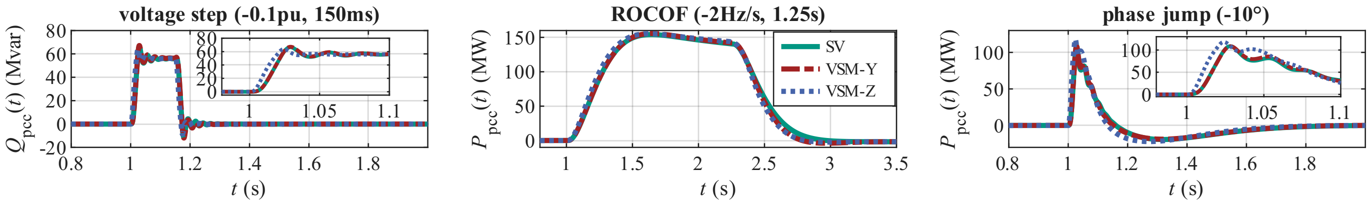

Fig. 2: Validation of GFM behavior and similar response in time domain for all three GFM control approaches; left: voltage magnitude step of -0.1 pu for 150 ms, middle: frequency ramp with a rate of change of frequency (ROCOF) of -2 Hz/s for 1.25 s, right: voltage phase jump of -10°; measured following *DIN EN IEC 61400-21-1*

machine and determining the virtual rotor angle ϑ [6], [22]. However, the coupling terms like in the SV approach between active (APC) and reactive power control (RPC) are not considered leading to an independent active and reactive power control. The reactive power controller consists solely of a PI controller and a voltage feedforward. Further, a PLL is used to resynchronize the virtual rotor. In case of the VSM-Y approach, the virtual admittance Y_{virt} in combination with the notch filter is also used as virtual stator representation transforming e_{d} to $i_{\mathrm{ref},dq}$ (see [7]).

3) VSM-Z: The VSM approach including a virtual impedance Z_{virt} instead of a virtual admittance Y_{virt} is based on the control approach of [6] and [19]. Here, the VSM itself with the APC and RPC is the same as of the VSM-Y approach, but e_{d} is subsequently transformed by Z_{virt} to the reference voltage $v_{\mathrm{ref},dq}$, which functions as input of the consecutive voltage control VC. Latter consists of a proportional gain and a current feedforward, with $i_{\mathrm{ref},dq}$ as manipulated variable.

III. Validation in time domain

The three different GFM control implementations are identically parameterized with respect to the outer control loops, the current controller (CC) and filters they have in common, while Y_{virt} and the notch filter, as well as Z_{virt} and the VC, respectively, are tuned such that they exhibit similar and comparable disturbance response. To validate the equivalence of their behavior three GFM scenarios meant for validation of GFM behavior have been chosen:

- a voltage step of -0.1 pu for 150 ms at PCC
- a voltage phase jump of -10° at PCC
- a change of frequency of -2 Hz/s for 1.25 s at PCC

All simulations are conducted in *PSCAD/EMTDC* at an operating point of $P = 0\,\mathrm{MW}$ and $Q = 0\,\mathrm{Mvar}$.

Figure 2 shows the response in reactive and active power of the considered GFM approaches for all three scenarios, respectively. Here, all three approaches show similar behavior for the considered scenarios validating a comparable time domain behavior. Additionally, their GFM behavior for these scenarios has been ensured.

IV. Impedance scan results

The frequency-dependent impedance is determined by means of a stepwise impedance scan in EMT software. Here, the focus lies on the SISO (single-input single-output) impedance, i.e. the impedance in the positive sequence domain (PSD) is determined for a PSD perturbation and the impedance in the negative sequence domain (NSD) for a NSD perturbation. For the perturbation, an additional voltage with the considered perturbation frequency and an amplitude of 2 % of the rated grid voltage amplitude is added to the grid voltage.

A. Comparison and overview of the GFM control approaches

In a first step, the PSD and NSD impedance of each control approach is determined. Figure 3 depicts a comparison of the frequency-dependent impedances of all three E-STATCOMs with the respective GFM control variant. Here, a very good accordance of the SV and the VSM-Y approach can be observed, indicating a dominating influence of the virtual admittance Y_{virt}, while the impact of the implementation of the SV and the VSM itself is negligible. This observation supports the findings of [7]. In PSD, especially the 360° phase turn between 50 Hz and 110 Hz stands out suggesting a non-passivity between 55 Hz and 90 Hz. Further, an active behavior for frequencies $f < 8\,\mathrm{Hz}$ is observable. In the NSD impedance, an undesired non-passivity between 20 Hz and 50 Hz is apparent. On the contrary, the VSM-Z approach exhibits an impedance differing from the SV or the VSM-Y approach up to a frequency of $f{=}3\,\mathrm{kHz}$. Here, the only non-passivity is located in the PSD impedance in the frequency range of $55\,\mathrm{Hz} \leq f \leq 200\,\mathrm{Hz}$. Further, the 360° phase shift as noted for the SV or VSM-Y impedance is not observable. In the NSD, the VSM-Z impedance remains in the passive region across the entire frequency range. The differences between VSM-Y and VSM-Z underline the impact of the implementation of the virtual stator representation, i.e. the usage of Y_{virt} or Z_{virt}.

B. Influence of the notch filter

Since the main difference in the frequency-dependent impedance of VSM-Z, VSM-Y and SV is related to the virtual impedance and admittance as well as the notch filter, the focus in this section lies on differentiating the influence of Y_{virt} and the notch filter. For this, the impact of the notch filter on the frequency-dependent impedance is investigated. Figure 4 compares the VSM-Y approach already examined with the notch filter to a VSM-Y approach omitting the notch filter. Additionally, the results of the virtual impedance of VSM-Z are plotted for reference. It can be seen that the magnitude of the impedance is significantly increased at $f \approx 100\,\mathrm{Hz}$ without the notch filter, indicating a resonance at this frequency. Further, omitting the notch filter widens the frequency range of the 360° phase shift in the PSD impedance, resulting in a non-passivity reaching over 100 Hz. Therefore, the phase shift does not solely originate from the notch filter. It could

979-8-3315-8138-1

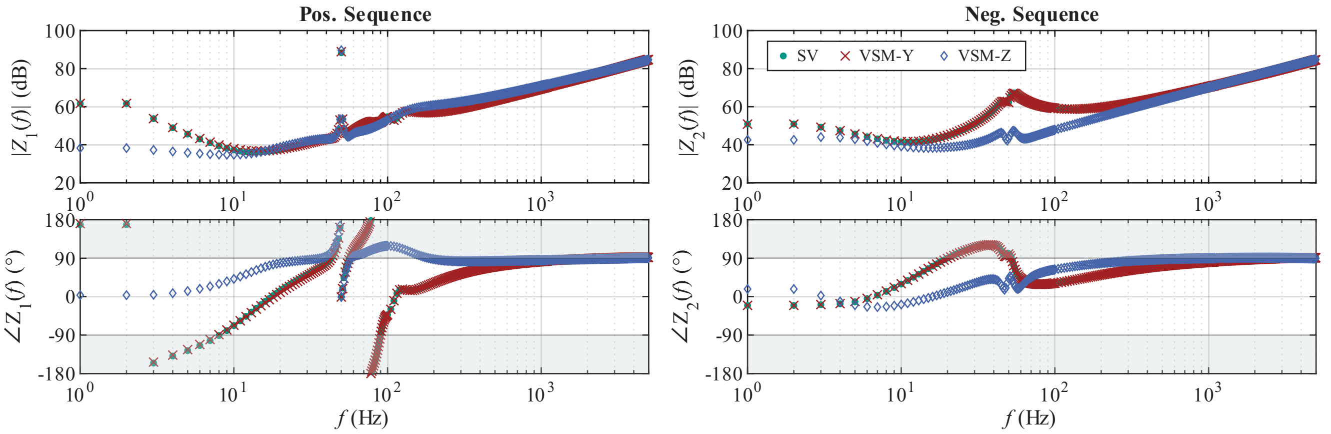

Fig. 3: Positive and negative sequence impedance of the considered E-STATCOM with a SV, a VSM-Y and a VSM-Z approach

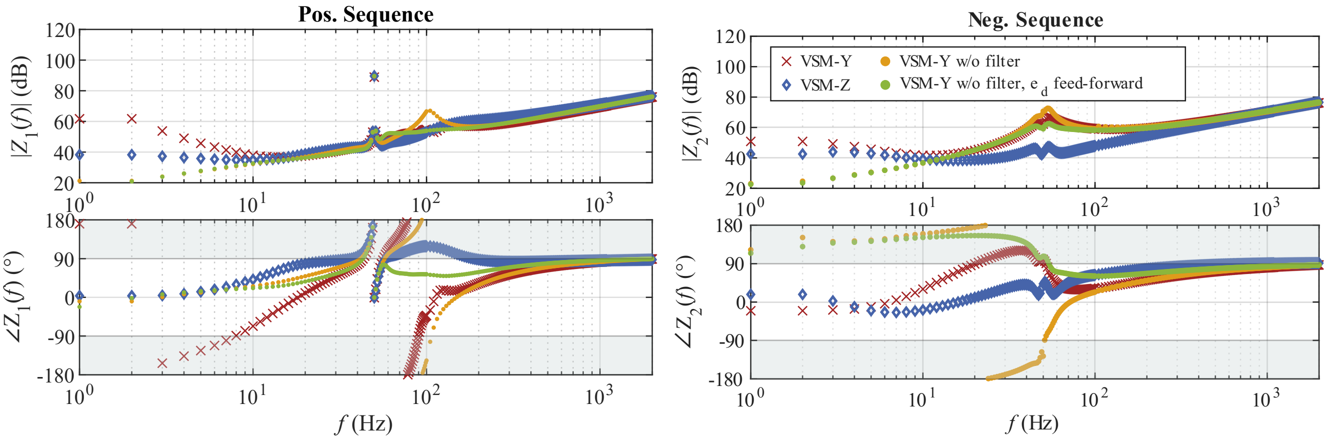

Fig. 4: Influence of the notch filter and the voltage feedforward on the positive and negative sequence impedance for the VSM-Y approach

eventually be traced back to the feedback of $v_{\mathrm{T},dq}$ to Y_{virt} and the feedforward of $v_{\mathrm{T},dq}$ in the CC. Replacing $v_{\mathrm{T},dq}$ with e_{d} averts the phase shift and the converter stays passive at this frequency range, see green dotted line in Fig. 4.

For low frequencies $f < 10\,\mathrm{Hz}$ considering VSM-Y without notch filter, the phase remains in the passive region similar to the VSM-Z approach. Additionally, the magnitude in this frequency range is clearly reduced in comparison to the VSM-Y with notch filter. In the NSD, omitting the filter results contrarily in a non-passivity for frequencies $f < 50\,\mathrm{Hz}$. These differences are a consequence of the notch filter being implemented in the *dq* frame resulting in filtering and phase shifting around 50 Hz in *dq*, and hence, an influence in PSD at 100 Hz as well as in NSD at 0 Hz. Especially, the filtering and the phase shift around 0 Hz are visible in both PSD and NSD due to the bandwidth of the filter. Figure 5 validates this. Here, the impact of the bandwidth of the notch filter in terms of the Q factor on the frequency-dependent impedance is visible. The higher the bandwidth of the filter, i.e. the lower its Q factor, the broader the frequency range of influence. Further, it can be seen that a notch filter with a higher bandwidth can reduce or even avoid the non-passivity in the NSD, but it increases the crossing frequency of the active region at lower frequencies in the PSD. However, it should be noted that a higher bandwidth results in a reduced dynamic in the time domain.

C. Discussion of impedance scan results

In light of the German Technical Requirements for grid-forming assets [12], demanding a passive behavior for frequencies $f > 10\,\mathrm{Hz}$ and especially for frequencies in the range of $100\,\mathrm{Hz} < f < 1\,\mathrm{kHz}$, each approach exhibits its advantages and disadvantages.

The impedance of VSM-Z contains a non-passivity up to 200 Hz violating the requirements for $f > 100\,\mathrm{Hz}$ clearly. However, the non-passivity in this frequency range can be influenced and shifted by changing the inertia constant as shown in [23]. Further, below 40 Hz in the PSD and within the entire considered frequency range in the NSD the impedance remains passive.

In case of SV and VSM-Y, there is no non-passivity for frequencies in the range of $100\,\mathrm{Hz} < f < 1\,\mathrm{kHz}$ and hence, meets the requirements for this frequency range better than the VSM-Z approach. However, the impedance exhibits for frequencies below $f < 10\,\mathrm{Hz}$ clearly an active behavior in the PSD and further, a non-passivity between 20 Hz and 50 Hz in the NSD, violating the requirements in a frequency range where the VSM-Z approach fulfills them. Here, omitting the notch filter avoids the active region in the PSD, but leads to an active behavior of the VSM-Y and SV approach for frequencies below $f < 50\,\mathrm{Hz}$ in the NSD. Therefore, Y_{virt} with and without the notch filter leads to a non-passivity

979-8-3315-8138-1

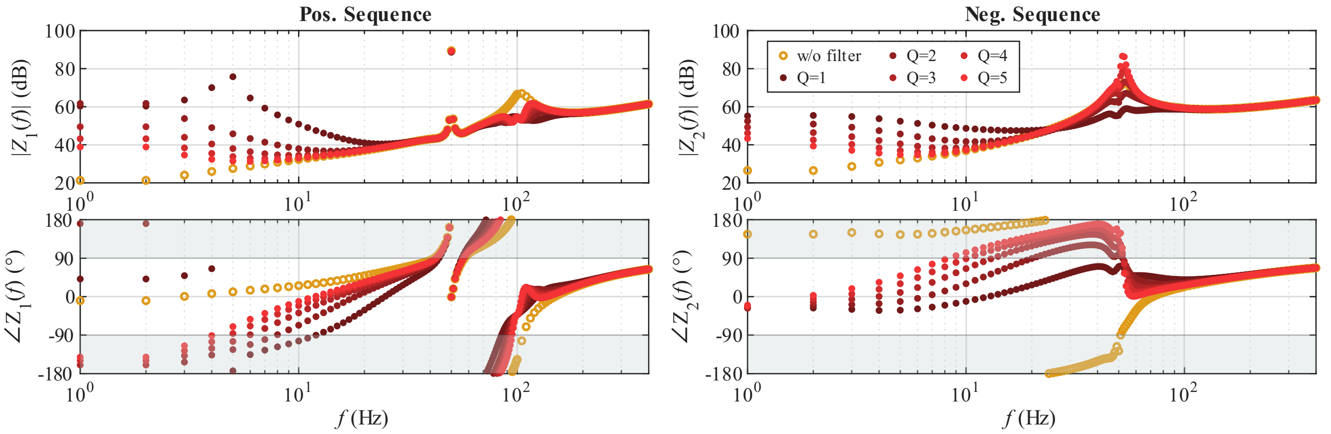

Fig. 5: Influence of the Q factor of the notch filter on the positive and negative sequence impedance, here in case for the VSM-Y approach

in the lower frequency range, in either PSD or NSD. The cause has not yet been identified and is the subject of further investigation.

V. Conclusion

This contribution investigated and compared three different grid-forming control approaches regarding their harmonic stability characteristics by means of their respective frequency-dependent impedance. All three approaches have been implemented for an E-STATCOM in EMT simulation software and subsequently analyzed by means of an impedance scan and a passivity-based stability analysis. Here, the impedance of the SV and the VSM-Y approach match very well, while the impedance of the VSM-Z approach differs notably. Especially, the feedback of the measured ac voltage in the virtual admittance combined with the voltage feedforward of the current control has a great impact on the frequency-dependent impedance, leading to a 360° phase shift between 50 Hz and 100 Hz. Adding a notch filter in *dq* domain filtering the virtual admittance output reduces the bandwidth of the 360° phase shift, but affects the passivity at subsynchronous frequencies significantly in both positive and negative sequence domain.

References

[1] M. Chandorkar, D. Divan, and R. Adapa, "Control of parallel connected inverters in standalone AC supply systems," *IEEE Trans. Ind Appl.*, vol. 29, pp. 136–143, Jan. 1993.

[2] A. Tayyebi, F. Dörfler, F. Kupzog, Z. Miletic, and W. Hribernik, "Grid-forming converters – inevitability, control strategies and challenges in future grids application," *CIRED Workshop*, no. 0236, 2018.

[3] I. Cvetkovic, D. Boroyevich, R. Burgos, C. Li, and P. Mattavelli, "Modeling and control of grid-connected voltage-source converters emulating isotropic and anisotropic synchronous machines," in *2015 IEEE 16th Workshop on Contr. and Modeling for Power Electron. (COMPEL)*, pp. 1–5, July 2015.

[4] C. Arghir, T. Jouini, and F. Dörfler, "Grid-forming control for power converters based on matching of synchronous machines," *Automatica*, vol. 95, pp. 273–282, Sept. 2018.

[5] S. D'Arco and J. A. Suul, "Equivalence of Virtual Synchronous Machines and Frequency-Droops for Converter-Based MicroGrids," *IEEE Trans. Smart Grid*, vol. 5, pp. 394–395, Jan. 2014.

[6] C. Hirsching, M. Goertz, S. Wenig, A. Bisseling, M. Suriyah, and T. Leibfried, "On Fault-Ride-Through Performance in MMC-HVDC Applications Controlled as a Virtual Synchronous Machine," *IEEE Trans. Energy Convers.*, vol. 37, pp. 2803–2812, Dec. 2022.

[7] P. Weber, A. Bisseling, L. Hörmann, M. Suriyah, and T. Leibfried, "Comparative analysis of a virtual synchronous machine and a synchronverter based on grid-forming benchmark scenarios," in *23rd Wind & Solar Integration Workshop (WIW 2024)*, pp. 556–563, Oct. 2024.

[8] Q.-C. Zhong and G. Weiss, "Synchronverters: Inverters that mimic synchronous generators," *IEEE Trans. Ind. Electron.*, vol. 58, pp. 1259–1267, Apr. 2011.

[9] W. Schulze, P. Weber, M. Suriyah, and T. Leibfried, "Grid-forming synchronverter-based control method with current limiting method for grid-side converters of converter-based generation plants," in *21st Wind & Solar Integr. Workshop (WIW 2022)*, pp. 394–401, Oct. 2022.

[10] P. Weber, W. Schulze, P. Pawlowski, M. Suriyah, and T. Leibfried, "Grid-forming synchronverter-based control method with current limiting method for grid-side converters of type 4 wind power plants," in *22nd Wind and Solar Integr. Workshop (WIW 2023)*, (Copenhagen), pp. 422–429, Sept. 2023.

[11] A. Bisseling, P. Weber, D. Bohn, M. Suriyah, and T. Leibfried, "EMT simulation of an IEEE 9-bus benchmark-model adapted to European transmission grid standards with 100% inverter-based resources," in *23rd Wind & Solar Integr. Workshop (WIW 2024)*, pp. 572–579, Oct. 2024.

[12] VDE FNN Hinweis, "Technische Anforderungen an Netzbildende Eigenschaften inklusive der Bereitstellung von Momentanreserve," 2025.

[13] M. Lindner, H. Abele, C. John, and J. Lehner, "Suitable Classification of Power System Stability Phenomena,"

[14] Cigré WG C4.49, "TB928: Multi-frequency stability of converter-based modern power systems," 2024.

[15] Cigré WG B4.67, "TB754: AC side harmonics and appropriate harmonic limits for VSC HVDC," 2019.

[16] L. Harnefors, X. Wang, A. G. Yepes, and F. Blaabjerg, "Passivity-Based Stability Assessment of Grid-Connected VSCs—An Overview," *IEEE J. Emerg. Sel. Top. Ind. Electron.*, vol. 4, pp. 116–125, Mar. 2016.

[17] J. Sun, "Impedance-Based Stability Criterion for Grid-Connected Inverters," *IEEE Trans. Power Electron.*, vol. 26, pp. 3075–3078, Nov. 2011.

[18] J. Segundo-Ramirez, A. Bayo-Salas, M. Esparza, J. Beerten, and P. Gómez, "Frequency Domain Methods for Accuracy Assessment of Wideband Models in Electromagnetic Transient Stability Studies," *IEEE Trans. Power Del.*, vol. 35, pp. 71–83, Feb. 2020.

[19] A. Bisseling, C. Hirsching, K. Haeusler, M. Suriyah, and T. Leibfried, "Impact of supercapacitor energy storage on transient behaviour of MMC-based grid-forming ES-STATCOM," in *23rd Int. Symp. on High Voltage Eng. (ISH 2023)*, vol. 2023, pp. 92–98, 2023.

[20] Cigré WG B4.57, "TB604: Guide for the Development of Models for HVDC Converters in a HVDC Grid," 2014.

[21] T. Younis, M. Ismeil, E. K. Hussain, and M. Orabi, "Improved single-phase self-synchronised synchronverter with enhanced dynamics and current limitation capability," *IET Power Electronics*, vol. 12, no. 2, pp. 337–344, 2019.

[22] S. D'Arco, G. Guidi, and J. A. Suul, "Operation of a Modular Multilevel Converter Controlled as a Virtual Synchronous Machine," in *2018 Int. Power Electron. Conf. (IPEC-Niigata 2018)*, pp. 782–789, May 2018.

[23] C. Hirsching, M. Lindner, A. Bisseling, M. Suriyah, and T. Leibfried, "Control Structure Related Admittance-Shaping Effects in VSM Controlled Converters," in *2022 IEEE PES Innovative Smart Grid Technologies - Asia (ISGT Asia)*, pp. 130–134, Nov. 2022.

979-8-3315-8138-1